IEEE Access
Multidisciplinary | Rapid Review | Open Access Journal

Received 7 December 2023, accepted 23 December 2023, date of publication 28 December 2023,
date of current version 5 January 2024.

Digital Object Identifier 10.1109/ACCESS.2023.3347807

RESEARCH ARTICLE

Singularity-Free Fixed-Time Neuro-Adaptive Control for Robot Manipulators in the Presence of Input Saturation and External Disturbances

DONG GUO[1,3], JUN LIU[2], SONG ZHENG[1], JIAN-PING CAI[3], AND PENG JIANG[2]
[1]School of Automation (Artificial Intelligence), Hangzhou Dianzi University, Hangzhou 310005, China
[2]School of Information Science and Technology, Hangzhou Normal University, Hangzhou 310030, China
[3]College of Electrical Engineering, Zhejiang University of Water Resources and Electric Power, Hangzhou 310018, China

Corresponding author: Peng Jiang (pjiang19751030@163.com)

This work was supported in part by the National Natural Science Foundation of China under Grant 62273126, in part by the Ling-Yan Research and Development Project of Zhejiang Province of China under Grant 2023C03185, and in part by the Zhejiang Provincial Natural Science Foundation of China under Grant LQ21F030012 and Grant LY22F030011.

ABSTRACT This article proposes a singularity-free fixed-time neuro-adaptive control strategy for robot manipulators, with the goal of addressing trajectory-tracking challenges presented by model uncertainties, external disturbances, and input saturation. To mitigate the impact of input saturation, an auxiliary system is introduced. Combining the backstepping technique, a fixed-time neuro-adaptive controller is designed to ensure that tracking errors converge within a small region around the origin within a fixed time, with the upper bound of convergence time being independent of initial conditions. Notably, the direct avoidance of singularity is achieved by constructing quadratic-fraction functions in both the virtual controller and the actual controller, eliminating the need for filters or piecewise continuous functions. This simplifies and streamlines the stability analysis process. To validate the effectiveness of this strategy, numerical simulations are conducted.

INDEX TERMS Robot manipulators, adaptive control, fixed-time convergence, neural network, input saturation.

I. INTRODUCTION

Robot manipulators have received extensive applications across industries such as manufacturing, medical treatment, cargo handling, and space exploration, contributing significantly to enhanced automation and efficiency. Within the realm of robot manipulator dynamics, intricate inherent attributes come into play, including load fluctuations, hysteresis, friction, and coupling. These intricacies impart a challenging and multifaceted nature to the control aspects, requiring sophisticated and nuanced solutions. To this end, advanced control strategies have been proposed over the past few decades. These strategies encompass a wide range of approaches, including decentralized control [1], feedback linearization [2], PID control [3], H_∞ control [4], robust control [5], neural network and fuzzy system [6], [7], and sliding mode control(SMC) [8]. In the aforementioned literatures [1], [2], [3], [4], [5], [6], [7], and [8], it has been demonstrated that these control methods achieve asymptotic convergence of position tracking errors, signifying that the convergence time is infinite.

As widely acknowledged, convergence performance serves as a pivotal metric for evaluating system quality. In recent years, there has been significant progress in enhancing the convergence speed of systems through the development of finite-time control methods [9]. Finite-time control guarantees that system errors converge to an equilibrium point or a neighborhood around it within a finite time, making it a widely adopted approach in various nonlinear systems [10], [11], [12], [13], [14], [15], [16], [17].

The associate editor coordinating the review of this manuscript and approving it for publication was Nasim Ullah.

Yu et al. [15] introduced a continuous finite-time control scheme based on the terminal sliding mode surface (TSMC) for rigid robot manipulators, aiming to achieve faster and highly precise tracking performance. Luan et al. [16] presented an adaptive neural finite-time control strategy for nonlinear robot manipulators by incorporating the sliding mode technique into the design of adaptive laws and feedback control. Zhai and Xu [17] devised a novel non-singular terminal sliding mode controller to address the trajectory tracking challenge in robot manipulators affected by internal uncertainties and external disturbances, ensuring global state convergence to the origin within a finite time. Nevertheless, it is important to note that the convergence time in the literatures [9], [10], [13], [14], [15], [16], and [17] depends on the system's initial conditions, implying that the convergence time may vary under different initial conditions.

To amend the weakness of finite-time control, the concept of fixed-time stability was initially introduced by Polyakov [18], where the upper bound of the settling time became independent of initial conditions. Due to its notable advantages, fixed-time control schemes have been documented in the context of various nonlinear systems [19], [20], [21], [22]. For instance, Zuo [19] investigated the fixed-time consensus tracking problem for second-order multi-agent systems in networks with directed topology. Chen et al. [20] devised an adaptive nonsingular fixed-time sliding mode controller to address the attitude stabilization of uncertain rigid spacecraft coping with inertia uncertainties, external disturbance and actuator saturation. Van and Ceglarek [21] proposed a robust fixed-time fault-tolerant control strategy for robot manipulators, which combines a fixed-time second-order sliding mode observer and a fixed-time sliding mode control design approach. Zhang et al. [22] introduced an adaptive fault-tolerant approach with a fixed-time sliding mode for trajectory tracking of uncertain robot manipulators afflicted by actuator effectiveness faults. However, it's worth noting that many of the aforementioned finite and fixed-time control strategies [15], [16], [17], [18], [19], [20], [21], [22] were grounded in sliding mode control, which can potentially lead to undesirable chattering. As is well known, the singularity problem has become a common problem in fixed-time control design. Thus, this problem should be released during the control design for robot manipulators because it can lead to unbounded control torque and even the instability of robot manipulator systems. Moreover, these fixed-time control schemes typically address the singularity problem by incorporating piecewise continuous functions. In contrast, aside from sliding mode control, the backstepping design represents an alternative technique to achieve fixed-time control performance. A fixed-time backstepping control approach has been developed by integrating command filtered control and disturbance observer to tackle the trajectory tracking problem in surface vehicles [23]. However, the inclusion of a command filter may introduce challenges in stability analysis. As far as current knowledge is concerned, the task of designing a singularity-free fixed-time backstepping controller without relying on filters or piecewise continuous functions remains a challenging endeavor.

In addition, to address the inherent uncertainties in the system dynamics, two prominent artificial intelligence techniques, namely neural networks (NNs) and fuzzy logic systems (FLSs), have been integrated into the controller design (refer to [24], [25], [26], [27], [28], [29] and the related references). He et al. [28] introduced an adaptive neural network control approach for solving the tracking control problem of uncertain n-link robots, where neural networks were harnessed to effectively manage system uncertainties and disturbances. Wang et al. [29] devised a neural network-based terminal sliding-mode control scheme for robot manipulators, encompassing actuator dynamics, with the utilization of radial basis function neural networks to approximate the nonlinear dynamics of the robot manipulator. However, it should be noted that the literature mentioned above [28], [29] only guarantees either asymptotic or finite-time convergence of trajectory errors.

Inspired by the preceding discussions, this article presents a singularity-free fixed-time neuro-adaptive control (SFFTNAC) strategy for robot manipulators aimed at addressing the challenges of position tracking in the presence of model uncertainties, external disturbances, and input saturation. The primary objective is to ensure that tracking errors converge to the vicinity of the origin within a fixed time. The main contributions of this article can be summarized as follows.

1) In contrast to the existing finite-time control strategies [10], [11], [12], [13], [14], [15], [16], [17], this article systematically introduces a fixed-time backstepping control approach. This approach ensures that the trajectory tracking error converges to a compact region around the origin within a fixed time, with the upper bound of convergence time being independent of initial conditions.

2) Different from the existing fixed-time control strategies [21], [22], [23], this article presents a novel approach that incorporates quadratic-fraction function forms in controller design. This innovative design circumvents the singularity problem caused by the differentiation of the virtual controller without the necessity of filters or piecewise continuous functions, thereby simplifying the controller design process.

3) An auxiliary system is constructed to mitigate the effects of input saturation, and neural networks are employed to approximate the lumped uncertainty of the robot manipulator system. The practical fixed-time stability of the overall system is rigorously established through the use of Lyapunov theory.

II. PROBLEM FORMULATION AND PRELIMINARIES

A. PROBLEM FORMULATION

A class of n-link robotic manipulators are considered in this article, whose system dynamics may be described as follows [15]:

$$\boldsymbol{M}(\boldsymbol{q})\ddot{\boldsymbol{q}} + \boldsymbol{C}(\boldsymbol{q}, \dot{\boldsymbol{q}})\dot{\boldsymbol{q}} + \boldsymbol{G}(\boldsymbol{q}) = \boldsymbol{u} + \boldsymbol{d} \tag{1}$$

TABLE 1. Definitions of symbols in robotic dynamics.

Symbol	Definition
$\boldsymbol{q}$	the vector of joint angular position
$\boldsymbol{M}(\boldsymbol{q})$	a symmetric positive definite inertia matrix
$\boldsymbol{C}(\boldsymbol{q},\dot{\boldsymbol{q}})$	the vector of centripetal and Coriolis torques
$\boldsymbol{G}(\boldsymbol{q})$	the gravitational force
$\boldsymbol{d}$	sum of model uncertainties and external disturbances
$\boldsymbol{u}$	the constrained input

in which, $\boldsymbol{q} = [q_1, q_2, \cdots, q_n]^T \in \mathbb{R}^n$, $\boldsymbol{M}(\boldsymbol{q}) \in \mathbb{R}^{n\times n}$, $\boldsymbol{C}(\boldsymbol{q},\dot{\boldsymbol{q}}) \in \mathbb{R}^{n\times n}$, $\boldsymbol{G}(\boldsymbol{q}) \in \mathbb{R}^n$, $\boldsymbol{d} = [d_1, d_2, \cdots, d_n]^T \in \mathbb{R}^n$, $\boldsymbol{u} = [u_1, u_2, \cdots, u_n]^T \in \mathbb{R}^n$, and the definitions of above symbols are shown in Table 1.

Affected for saturation, the elements in $\boldsymbol{u}$ are formulated as follows: For $i = 1, \cdots, n$,

$$u_i = \text{sat}(v_i) = \begin{cases} \text{sgn}(v_i)u_{i\max}, & |v_i| \geq u_{i\max} \\ v_i, & |v_i| < u_{i\max}, \end{cases} \tag{2}$$

where v_i is the actual control input to be designed later, and $u_{i\max}$ is the maximum allowable torque. To streamline the analysis, a smooth function is adopted to approximate the saturation function. Define $\boldsymbol{v} = [v_1, v_2, \cdots, v_n]^T \in \mathbb{R}^n$ and $\boldsymbol{g}(\boldsymbol{v}) = [g_1(v_1), \ldots, g_n(v_n)]^T$, where $g_i(v_i)(i = 1, \ldots, n)$ is a smooth function as follows:

$$g_i(v_i) = u_{i\max} \times \tanh\Big(\frac{v_i}{u_{i\max}}\Big) = u_{i\max}\frac{e^{\frac{v_i}{u_{i\max}}} - e^{\frac{-v_i}{u_{i\max}}}}{e^{\frac{v_i}{u_{i\max}}} + e^{\frac{-v_i}{u_{i\max}}}}. \tag{3}$$

By letting $\boldsymbol{d}_s(\boldsymbol{v}) = [d_{s1}(v_1), \ldots, d_{sn}(v_n)]^T$, in which $d_{si}(v_i) = \text{sat}(v_i) - g_i(v_i)$, for $i = 1, \cdots, n$, we can deduce that

$$\boldsymbol{u} = \boldsymbol{g}(\boldsymbol{v}) + \boldsymbol{d}_s(\boldsymbol{v}). \tag{4}$$

It is easy to see that the following property holds:

For $i = 1, \cdots, n$,

$$|d_{si}(v_i)| \leq u_{i\max}(1 - \tanh(1)) \triangleq D. \tag{5}$$

Define

$$\begin{cases} \Delta\boldsymbol{M}(\boldsymbol{q}) = \boldsymbol{M}(\boldsymbol{q}) - \boldsymbol{M}_0(\boldsymbol{q}), \\ \Delta\boldsymbol{C}(\boldsymbol{q},\dot{\boldsymbol{q}}) = \boldsymbol{C}(\boldsymbol{q},\dot{\boldsymbol{q}}) - \boldsymbol{C}_0(\boldsymbol{q},\dot{\boldsymbol{q}}), \\ \Delta\boldsymbol{G}(\boldsymbol{q}) = \boldsymbol{G}(\boldsymbol{q}) - \boldsymbol{G}_0(\boldsymbol{q}), \end{cases} \tag{6}$$

where $\boldsymbol{M}_0(\boldsymbol{q})$, $\boldsymbol{C}_0(\boldsymbol{q},\dot{\boldsymbol{q}})$ and $\boldsymbol{G}_0(\boldsymbol{q})$ are the nominal components of robotic systems. It follows from (6) and (1) that

$$\boldsymbol{M}_0(\boldsymbol{q}) + \boldsymbol{C}_0(\boldsymbol{q},\dot{\boldsymbol{q}}) + \boldsymbol{G}_0(\boldsymbol{q}) = \boldsymbol{u} + \boldsymbol{d}_\Sigma + \boldsymbol{d}, \tag{7}$$

where $\boldsymbol{d}_\Sigma = \Delta\boldsymbol{M}(\boldsymbol{q})\ddot{\boldsymbol{q}} - \Delta\boldsymbol{C}(\boldsymbol{q},\dot{\boldsymbol{q}})\dot{\boldsymbol{q}} - \Delta\boldsymbol{G}(\boldsymbol{q})$. By letting $\boldsymbol{x}_1 = \boldsymbol{q}, \boldsymbol{x}_2 = \dot{\boldsymbol{q}}$, it can be inferred from (7) that

$$\begin{cases} \dot{\boldsymbol{x}}_1 = \boldsymbol{x}_2, \\ \dot{\boldsymbol{x}}_2 = \boldsymbol{M}_0^{-1}(\boldsymbol{x}_1)\big[\boldsymbol{d}_\Sigma + \boldsymbol{u} - \boldsymbol{C}_0(\boldsymbol{x}_1,\boldsymbol{x}_2)\boldsymbol{x}_2 - \boldsymbol{G}_0(\boldsymbol{x}_1)\big]. \end{cases} \tag{8}$$

The control objective of this article is to design a fixed-time neuro-adaptive controller $\boldsymbol{v}$ for the manipulator with uncertainties and external disturbances, such that $\boldsymbol{x}_1$ can track the reference trajectory $\boldsymbol{x}_d$ during a fixed time. The robot dynamics given in (1) satisfies the following assumptions:

Assumption 1: [30] There exist two unknown constant ι_1 and ι_2, such that

$$\ell_1 I \leq \boldsymbol{M}(\boldsymbol{q}) \leq \ell_2 I, \tag{9}$$

where I is a n-dimensional identity matrix.

Assumption 2: [30] The unknown time-varying disturbance $\boldsymbol{d}$ is assumed to be bounded, and there exists an unknown positive constant D' such that $||\boldsymbol{d}|| \leq D'$.

Remark 1: From the perspective of practical engineering, the position $\boldsymbol{q}$, velocity $\dot{\boldsymbol{q}}$ and acceleration $\ddot{\boldsymbol{q}}$ are bounded due to the mechanic limitations or the task space limitations of the space manipulator [31]. Moreover, the disturbance $\boldsymbol{d}$ is bounded, and $\boldsymbol{M}(\boldsymbol{q})$, $\boldsymbol{C}(\boldsymbol{q},\dot{\boldsymbol{q}})$, $\boldsymbol{G}(\boldsymbol{q})$ are continuous functions of the coordinates $\boldsymbol{q}$ and $\dot{\boldsymbol{q}}$. Thus, it is reasonable to assume that the lumpped uncertainty $\boldsymbol{d}_\Sigma$ is bounded.

B. PRELIMINARIES

Before the controller design, a definition and several lemmas are given as follows:

Definition 1: For $\zeta \in \mathbb{R}, \delta \in \mathbb{R}$,

$$\text{sig}^\zeta \delta \triangleq |\delta|^\zeta \cdot \text{sgn}(\delta), \tag{10}$$

and for $\zeta \in \mathbb{R}, \boldsymbol{\delta} = [\delta_1, \delta_2, \cdots, \delta_n]^T \in \mathbb{R}^n$,

$$\text{sig}^\zeta \boldsymbol{\delta} \triangleq [\text{sig}^\zeta \delta_1, \text{sig}^\zeta \delta_2, \cdots, \text{sig}^\zeta \delta_n]^T, \tag{11}$$

where $\text{sgn}(\cdot)$ represents the symbol of signum function.

Lemma 1: [20] Consider a scalar system $\dot{\chi} = f(\chi)$. For a continuous function $V(\chi)$, if there exist $0 < \gamma_1 < 1$, $\gamma_2 > 1$, $\alpha_1 > 0$, $\alpha_2 > 0$, and $\vartheta > 0$, such that

$$\dot{V}(\chi) \leq -\alpha_1 V^{\gamma_1} - \alpha_2 V^{\gamma_2} + \vartheta \tag{12}$$

holds, then the trajectory of the system $\dot{x} = f(\chi)$ is practical fixed-time stable, and the residual set of the solution is $\left\{\lim_{t\to T}\chi \;|\; V(\chi) \leq \min\left\{(\frac{\vartheta}{(1-\kappa)\alpha_1})^{\frac{1}{\gamma_1}}, (\frac{\vartheta}{(1-\kappa)\alpha_2})^{\frac{1}{\gamma_2}}\right\}\right\}$, where $0 < \kappa < 1$,

$$T \leq \frac{1}{\alpha_1}\frac{1}{\kappa(1-\gamma_1)} + \frac{1}{\alpha_2}\frac{1}{\kappa(\gamma_2 - 1)}. \tag{13}$$

Lemma 2: [32] For $\omega \in \mathbb{R}$ and $\epsilon \geq 0$, one can obtain

$$0 \leq |\omega| \leq \epsilon + \frac{\omega^2}{\sqrt{\omega^2 + \epsilon^2}}. \tag{14}$$

Lemma 3: [33] For $a \in \mathbb{R}, b \in \mathbb{R}$ the following inequality holds:

$$|a|^p|b|^q \leq \frac{p}{p+q}\delta|a|^{p+q} + \frac{q}{p+q}\delta^{-\frac{p}{q}}|b|^{p+q}, \tag{15}$$

where $p > 0$, $q > 0$ and $\delta > 0$.

Lemma 4: For $y \geq x$, and $\nu > 1$, the inequality

$$x(y-x)^\nu \leq \frac{\nu}{1+\nu}(y^{1+\nu} - x^{1+\nu}). \tag{16}$$

holds [34].

Lemma 5: [34] For $x_i \geq 0, i \in N^+$ and $\gamma > 0$, the following two inequalities hold:

$$\begin{cases} \sum_{i=1}^{n} x_i^{\gamma} \geq \left(\sum_{i=1}^{n} x_i\right)^{\gamma}, & \text{if} \quad 0 < \gamma < 1, \\ \sum_{i=1}^{n} x_i^{\gamma} \geq n^{1-\gamma}\left(\sum_{i=1}^{n} x_i\right)^{\gamma}, & \text{if} \quad \gamma > 1. \end{cases} \tag{17}$$

Lemma 6: [34] Consider the following differential equation as

$$\dot{\hat{\theta}}(t) = h_1\varphi(t) - h_2\hat{\theta}(t) - h_3\hat{\theta}^{\mu}(t), \tag{18}$$

where $h_1 > 0, h_2 > 0, h_3 > 0, \mu > 1$, and $\varphi(t)$ is a nonnegative function. If the initial value $\hat{\theta}(t_0) \geq 0$ holds, then $\hat{\theta}(t) \geq 0$ holds for $t \geq t_0$.

III. MAIN RESULTS

In this section, we will develop the neuro-adaptive fixed-time control law and then analyze the convergence of closed-loop robotic systems.

A. FIXED-TIME NEURO-ADAPTIVE CONTROL DESIGN

Step 1:

Define a Lyapunov function as follows:

$$V_1 = \frac{1}{2}z_1^T z_1, \tag{19}$$

where $\boldsymbol{z}_1 = [z_{1,1}, z_{1,2}, \cdots, z_{1,n}]^T = \boldsymbol{x}_1 - \boldsymbol{x}_d$ is the tracking error.

Differentiating (19) yields

$$\dot{V}_1 = z_1^T\dot{z}_1 = z_1^T(\dot{\boldsymbol{x}}_1 - \dot{\boldsymbol{x}}_d) = z_1^T z_2 + z_1^T\boldsymbol{\alpha} + z_1^T\boldsymbol{\eta}, \tag{20}$$

where $\boldsymbol{z}_2 = [z_{2,1}, z_{2,2}, \cdots, z_{1,n}]^T = \boldsymbol{x}_2 - \boldsymbol{\alpha} - \dot{\boldsymbol{x}}_d - \boldsymbol{\eta}$ is the intermediate error, $\boldsymbol{\eta} = [\eta_1, \ldots, \eta_n]^T$ is an auxiliary signal to be defined later, $\boldsymbol{\alpha}$ is the virtual controller given by

$$\boldsymbol{\alpha} = (\alpha_1, \alpha_2, \cdots, \alpha_n)^T, \tag{21}$$

where $\alpha_i (i = 1, 2, \cdots, n)$ is defined as

$$\alpha_i = -\frac{\bar{\alpha}_i(z_{1,i}\bar{\alpha}_i)}{\sqrt{(z_{1,i}^2\bar{\alpha}_i^2) + \varpi_1^2}}, \tag{22}$$

$$\bar{\alpha}_i = k_1 z_{1,i} + k_2 z_{1,i}^{\gamma_1} + k_3 z_{1,i}^{\gamma_2}, \tag{23}$$

where $0 < \gamma_1 < 1, \gamma_2 > 1, k_1 \geq 1, k_2 > 0, k_3 > 0, \varpi_1 > 0$, and the time derivative of α_i is given by

$$\dot{\alpha}_i = -\frac{d[\bar{\alpha}_i(z_{1,i}\bar{\alpha}_i)]/dt \cdot \sqrt{z_{1,i}^2\bar{\alpha}_i^2 + \varpi_1^2}}{z_{1,i}^2\bar{\alpha}_i^2 + \varpi_1^2} + \frac{\bar{\alpha}_i(z_{1,i}\bar{\alpha}_i) \cdot d\left[\sqrt{z_{1,i}^2\bar{\alpha}_i^2 + \varpi_1^2}\right]/dt}{z_{1,i}^2\bar{\alpha}_i^2 + \varpi_1^2} \tag{24}$$

where

$$d[\bar{\alpha}_i(z_{1,i}\bar{\alpha}_i)]/dt = 2\dot{\bar{\alpha}}_i z_{1,i}\bar{\alpha}_i + \bar{\alpha}_i^2\dot{z}_{1,i}, \tag{25}$$

$$d\left[\sqrt{z_{1,i}^2\bar{\alpha}_i^2 + \varpi_1^2}\right]/dt = \frac{1}{\sqrt{z_{1,i}^2\bar{\alpha}_i^2 + \varpi_1^2}} \times (z_{1,i}\dot{z}_{1,i}\bar{\alpha}_i^2 + z_{1,i}^2\bar{\alpha}_i\dot{\bar{\alpha}}_i) \tag{26}$$

and

$$\dot{\bar{\alpha}}_i = k_1\dot{z}_{1,i} + k_2\gamma_1 z_{1,i}^{\gamma_1 - 1}\dot{z}_{1,i} + k_3\gamma_2 z_{1,i}^{\gamma_2 - 1}\dot{z}_{1,i}. \tag{27}$$

By invoking (27), we have

$$z_{1,i}\dot{\bar{\alpha}}_i = k_1\dot{z}_{1,i}^2 + k_2\gamma_1 z_{1,i}^{\gamma_1}\dot{z}_{1,i} + k_3\gamma_2 z_{1,i}^{\gamma_2}\dot{z}_{1,i}. \tag{28}$$

From (28), we can see that the terms containing $z_{1,i}\dot{\bar{\alpha}}_i$ in (25) and (26) are nonsingular. Consequently, the singularity problem of the proposed virtual controller (22) is circumvented in a simpler way, which is different from some existing singularity-free design strategies, such as filters or piecewise continuous functions.

Remark 2: In (23), the virtual controller is designed in a quadratic-fraction form, which helps to avoid the occurrence of singularity problem. If the virtual controller is designed as follows:

$$\alpha_i = -(k_1 z_{1,i} + k_2\mathrm{sig}^{\gamma_1}(z_{1,i}) + k_3\,\mathrm{sig}^{\gamma_2}(z_{1,i})), \tag{29}$$

where $0 < \gamma_1 < 1, \gamma_2 > 1, k_1 \geq 1, k_2 > 0, k_3 > 0$. $\alpha_i = -\bar{\alpha}_i$. From (29), we can see that the singularity problem may occur in $\dot{\alpha}_i$ while $z_{1,i} = 0, \dot{z}_{1,i} \neq 0$, for the reason that $\gamma_1 - 1 < 0$.

Let $\bar{\boldsymbol{\alpha}} = (\bar{\alpha}_1, \bar{\alpha}_2, \cdots, \bar{\alpha}_n)^T$. Substituting (21), (22) into (20), by Lemma 2 and Lemma 5, we have

$$\begin{aligned} \dot{V}_1 &\leq z_1^T z_2 - z_1^T\bar{\boldsymbol{\alpha}} + z_1^T\boldsymbol{\eta} + \varpi_1 \\ &\leq ||\boldsymbol{z}_1||^2 + \frac{||\boldsymbol{z}_2||^2}{2} - k_1||\boldsymbol{z}_1||^2 - k_2||\boldsymbol{z}_1||^{1+\gamma_1} \\ &\quad - n^{\frac{1-\gamma_2}{2}}k_3||\boldsymbol{z}_1||^{1+\gamma_2} + \frac{||\boldsymbol{\eta}||^2}{2} + \varpi_1 \\ &\leq -\bar{k}_2 V_1^{\frac{1+\gamma_1}{2}} - \bar{k}_3 V_1^{\frac{1+\gamma_2}{2}} + \frac{||\boldsymbol{z}_2||^2}{2} + \frac{||\boldsymbol{\eta}||^2}{2} + \varpi_1. \end{aligned} \tag{30}$$

where $\bar{k}_2 = 2^{\frac{1+\gamma_1}{2}} \cdot k_2$ and $\bar{k}_3 = n^{\frac{1-\gamma_2}{2}}2^{\frac{1+\gamma_2}{2}} \cdot k_2$.

Step 2: Define another Lyapunov function as

$$V_2 = V_1 + \frac{1}{2}z_2^T z_2. \tag{31}$$

Differentiating (31) yields

$$\begin{aligned} \dot{V}_2 &= \dot{V}_1 + z_2^T(\dot{\boldsymbol{x}}_2 - \dot{\boldsymbol{\alpha}} - \ddot{\boldsymbol{x}}_d - \dot{\boldsymbol{\eta}}) \\ &= \dot{V}_1 + z_2^T\big[\boldsymbol{M}_0^{-1}(\boldsymbol{x}_1)(\boldsymbol{d}_\Sigma + \boldsymbol{d} + \boldsymbol{u} - \boldsymbol{C}_0(\boldsymbol{x}_1, \boldsymbol{x}_2)\boldsymbol{x}_2 \\ &\quad - \boldsymbol{G}_0(\boldsymbol{x}_1)) - \dot{\boldsymbol{\alpha}} - \ddot{\boldsymbol{x}}_d - \dot{\boldsymbol{\eta}}\big] \\ &= \dot{V}_1 + z_2^T\big[\boldsymbol{\Upsilon} + \boldsymbol{F} + \boldsymbol{M}_0^{-1}(\boldsymbol{x_1})\big(\boldsymbol{g}(\boldsymbol{v}) + \boldsymbol{d}_s(\boldsymbol{v})\big) - \dot{\boldsymbol{\eta}} + \boldsymbol{d}\big], \end{aligned} \tag{32}$$

where $\boldsymbol{F} = \boldsymbol{M}_0^{-1}(\boldsymbol{x}_1)\big(\boldsymbol{C}_0(\boldsymbol{x}_1, \boldsymbol{x}_2)\boldsymbol{x}_2 - \boldsymbol{G}_0(\boldsymbol{x}_1)\big) - \ddot{\boldsymbol{x}}_d$ and $\boldsymbol{\Upsilon} = \boldsymbol{M}_0^{-1}(\boldsymbol{x}_1)\boldsymbol{d}_\Sigma - \dot{\boldsymbol{\alpha}} = [\Upsilon_1, \Upsilon_2, \cdots, \Upsilon_n]^T$. According

to Assumption 2 and Remark 1, 111 Let us apply neural networks to approximate the uncertainty $\boldsymbol{\Upsilon}$ as followsc [37]:

$$\Upsilon_i = \boldsymbol{W}_i^{*T}\boldsymbol{\Phi}_i(\boldsymbol{Z}) + \varepsilon_i, i = 1, \ldots, n, \tag{33}$$

where $\boldsymbol{Z} = [\boldsymbol{x}_1^T, \boldsymbol{x}_2^T]^T$,

$$\boldsymbol{\Phi}_i(\boldsymbol{Z}) = \varsigma_1/(\varsigma_2 + \exp(-\boldsymbol{Z}/\varsigma_3)) + \varsigma_4, \tag{34}$$

$\boldsymbol{W}_i^*$ stands for the ideal weight of neural network, $\varsigma_1 > 0, \varsigma_2 > 0, \varsigma_3 > 0$ and $\varsigma_4 > 0$, and ε_i is the approximation error, which meets $|\varepsilon_i| \leq \varepsilon_N$ with ε_N being an unknown constant [35], [36],

Similar to *Step 1*, we design the actual control law as

$$\begin{aligned} \boldsymbol{v} &= -\boldsymbol{M}_0(\boldsymbol{x}_1)\boldsymbol{\rho}, \\ \boldsymbol{\rho} &= (\varrho_1, \varrho_2, \cdots, \varrho_n)^T \end{aligned} \tag{35}$$

where

$$\varrho_i = -\frac{\bar{v}_i(z_{2i}\bar{v}_i)}{\sqrt{(z_{2i}^2\bar{v}_i^2) + \varpi_2^2}}, i = 1, 2, \cdots, n, \tag{36}$$

and

$$\begin{aligned} (\bar{v}_1, \bar{v}_2, \cdots, \bar{v}_n)^T &= \lambda_1 z_2 + \lambda_2 sig^{\gamma_1}(z_2) + \lambda_3 sig^{\gamma_2}(z_2) \\ &+ \boldsymbol{F} + \frac{\hat{\theta}\boldsymbol{\chi} z_2}{2c_1^2} + \boldsymbol{\eta}, \end{aligned} \tag{37}$$

$\boldsymbol{\chi} = \text{diag}(\boldsymbol{\Phi}_1^T\boldsymbol{\Phi}_1, \ldots, \boldsymbol{\Phi}_n^T\boldsymbol{\Phi}_n)$ is a diagonal matrix, $\lambda_1 \geq 1$, $\lambda_2 > 0$, $\lambda_3 > 0$, $\varpi_2 \geq 0$, $h > 0$, $\theta = \max\{||\boldsymbol{W}_1^*||^2, \ldots, ||\boldsymbol{W}_n^*||^2\}$, and the parameter update law is designed as

$$\dot{\hat{\theta}} = \frac{c_2\sum_{i=1}^{n} z_{2i}^2\boldsymbol{\Phi}_i^T\boldsymbol{\Phi}_i}{2c_1^2} - c_3\hat{\theta} - c_4\hat{\theta}^{\gamma_2}, \hat{\theta}(0) = 0, \tag{38}$$

in which c_1, c_2, c_3, and c_4 are positive constants, and their recommended ranges are $0.2 \leq c_1 < 1$, $1 \leq c_2 \leq 10$, $0.1 \leq c_3 \leq 1$, and $0.1 \leq c_4 \leq 1$.

To deal with input saturation, we construct an auxiliary system as follows:

$$\dot{\boldsymbol{\eta}} = -\boldsymbol{\eta} + \left(\boldsymbol{M}_0^{-1}(\boldsymbol{x}_1)\boldsymbol{g}(\boldsymbol{v}) - \boldsymbol{M}_0^{-1}(\boldsymbol{x}_1)\boldsymbol{v}\right). \tag{39}$$

Substituting (35) and (39) into (32) yields

$$\begin{aligned} \dot{V}_2 \leq \dot{V}_1 &+ z_2^T\boldsymbol{F} + z_2^T\boldsymbol{\Upsilon} - z_2^T\bar{\boldsymbol{v}} + \varpi_2 + z_2^T\boldsymbol{\eta} \\ &+ z_2^T\boldsymbol{M}_0^{-1}(\boldsymbol{x}_1)\boldsymbol{d}_s(\boldsymbol{v}) + z_2^T\boldsymbol{d}, \end{aligned} \tag{40}$$

where $\bar{\boldsymbol{v}} = (\bar{v}_1, \bar{v}_2, \cdots, \bar{v}_n)^T$.

On the basis of Young's inequality, we have

$$\begin{aligned} z_2^T\boldsymbol{\Upsilon} &= \sum_{i=1}^{n} z_{2i}(\boldsymbol{W}_i^{*T}\boldsymbol{\Phi}_i + \varepsilon_i) \\ &\leq \sum_{i=1}^{n} |z_{2i}| \cdot |\boldsymbol{W}_i^{*T}\boldsymbol{\Phi}_i| + \sum_{i=1}^{n} |z_{2i}| \cdot \varepsilon_N \\ &\leq \frac{\theta\sum_{i=1}^{n} z_{2i}^2\boldsymbol{\Phi}_i^T\boldsymbol{\Phi}_i}{2c_1^2} + \frac{nc_1^2}{2} + \frac{||z_2||^2}{2} + \frac{n\varepsilon_N^2}{2}, \end{aligned} \tag{41}$$

$$z_2^T\boldsymbol{d} \leq \frac{||z_2||^2}{2} + \frac{||\boldsymbol{d}||^2}{2} \leq \frac{||z_2||^2}{2} + \frac{D'^2}{2} \tag{42}$$

and

$$z_2^T\boldsymbol{M}_0^{-1}(\boldsymbol{x}_1)\boldsymbol{d}_s(\boldsymbol{v}) \leq \frac{||z_2||^2}{2} + \frac{||\boldsymbol{M}_0^{-1}||^2D^2}{2}. \tag{43}$$

Substituting (30), (37), (41)-(43) into (40), we obtain

$$\begin{aligned} \dot{V}_2 \leq \dot{V}_1 &+ \frac{\tilde{\theta}\sum_{i=1}^{n} z_{2i}^2\boldsymbol{\Phi}_i^T\boldsymbol{\Phi}_i}{2c_1^2} + \frac{nc_1^2}{2} + ||z_2||^2 + \frac{n\varepsilon_N^2}{2} + \varpi_2 \\ &- \lambda_1||z_2||^2 - \lambda_2\left(\frac{1}{2}||z_2||^2\right)^{\frac{1+\gamma_1}{2}} - \lambda_3 n^{\frac{1-\gamma_2}{2}} \\ &\times \left(\frac{1}{2}||z_2||^2\right)^{\frac{1+\gamma_2}{2}} + \frac{D'^2}{2} \\ &\leq -\bar{\lambda}_2 V_2^{\frac{1+\gamma_1}{2}} - \bar{\lambda}_3 V_2^{\frac{1+\gamma_2}{2}} + \frac{\tilde{\theta}\sum_{i=1}^{3} z_{2i}^2\boldsymbol{\Phi}_i^T\boldsymbol{\Phi}_i}{2c_1^2} + \vartheta_1, \end{aligned} \tag{44}$$

where $\bar{\lambda}_2 = \min\{\bar{k}_2, \lambda_2 2^{\frac{1+\gamma_1}{2}}\}$, $\bar{\lambda}_3 = \min\{\bar{k}_3, \lambda_3 2^{\frac{1+\gamma_2}{2}} n^{\frac{1-\gamma_2}{2}}\}$, and $\vartheta_1 = \varpi_1 + \frac{nc_1^2}{2} + \frac{n\varepsilon_N^2}{2} + \varpi_2 + \frac{||\boldsymbol{M}_0^{-1}||^2D^2}{2} + \frac{||\boldsymbol{\eta}||^2}{2} + \frac{D'^2}{2}$.

B. PERFORMANCE ANALYSIS

Theorem 1: For the closed-loop robotic system composed of (8), fixed-time controller (35), parameter update law (38), and virtual control law (21), the tracking error $z_{1,i}$ can converge into the small neighborhood of origin within a fixed time.

Proof: Choose a Lyapunov function as follows:

$$V_3 = V_2 + \frac{1}{2c_2}\tilde{\theta}^2 \tag{45}$$

in which, $\tilde{\theta} = \theta - \hat{\theta}$. Taking the time derivative of V_3, we obtain

$$\begin{aligned} \dot{V}_3 &= \dot{V}_2 - \frac{1}{c_2}\tilde{\theta}\dot{\hat{\theta}} \\ &\leq -\bar{\lambda}_2 V_2^{\frac{1+\gamma_1}{2}} - \bar{\lambda}_3 V_2^{\frac{1+\gamma_2}{2}} + \vartheta_1 + \tilde{\theta}\left(\frac{\sum_{i=1}^{n} z_{2i}^2\boldsymbol{\Phi}_i^T\boldsymbol{\Phi}_i}{2c_1^2}\right. \\ &\left. - \frac{1}{c_2}\dot{\hat{\theta}}\right). \end{aligned} \tag{46}$$

Substituting (38) into (46) leads to

$$\dot{V}_3 \leq -\bar{\lambda}_2 V_2^{\frac{1+\gamma_1}{2}} - \bar{\lambda}_3 V_2^{\frac{1+\gamma_2}{2}} + \frac{c_3}{c_2}\tilde{\theta}\hat{\theta} + \frac{c_4}{c_2}\tilde{\theta}\hat{\theta}^{\gamma_2} + \vartheta_1. \tag{47}$$

Using the Young's inequality, we have

$$\frac{c_3}{c_2}\tilde{\theta}\hat{\theta} = \frac{c_3}{c_2}\tilde{\theta}(\theta - \tilde{\theta}) \leq -\frac{c_3\tilde{\theta}^2}{2c_2} + \frac{c_3\theta^2}{2c_2}. \tag{48}$$

Substituting (48) into (47) yields

$$\begin{aligned} \dot{V}_3 \leq -\bar{\lambda}_2 V_2^{\frac{1+\gamma_1}{2}} &- \bar{\lambda}_3 V_2^{\frac{1+\gamma_2}{2}} - \frac{c_3\tilde{\theta}^2}{2c_2} + \frac{c_3\theta^2}{2c_2} + \frac{c_4}{c_2}\tilde{\theta}\hat{\theta}^{\gamma_2} \\ &+ \vartheta_1. \end{aligned} \tag{49}$$

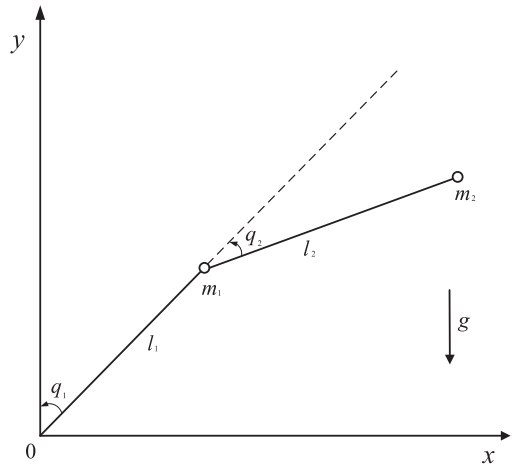

FIGURE 1. Configuration of a two-link robot manipulator.

By Lemma 3 and defining $a = 1, b = c_3\tilde{\theta}^2/(2c_2), p = \frac{1-\gamma_1}{2}, q = \frac{1+\gamma_1}{2}$ and $\delta = (\frac{2}{1+\gamma_1})^{\frac{1+\gamma_1}{\gamma_1-1}}$, we get

$$\left(\frac{c_3\tilde{\theta}^2}{2c_2}\right)^{\frac{1+\gamma_1}{2}} \leq \Theta(\gamma_1) + \frac{c_3\tilde{\theta}^2}{2c_2}, \tag{50}$$

where $\Theta(\gamma_1) = \frac{1-\gamma_1}{2} \times (\frac{2}{1+\gamma_1})^{\frac{1+\gamma_1}{\gamma_1-1}}$.

By Lemma 4 and Lemma 6, defining $x = \tilde{\theta}$ and $y = \theta$, we obtain

$$\tilde{\theta}\hat{\theta}^{\gamma_2} = \tilde{\theta}(\theta - \tilde{\theta})^{\gamma_2} \leq \frac{\gamma_2}{1+\gamma_2}(\theta^{1+\gamma_2} - \tilde{\theta}^{1+\gamma_2}). \tag{51}$$

Substituting (50) and (51) into (49), we have

$$\begin{aligned}\dot{V}_3 \leq & -\bar{\lambda}_2 V_2^{\frac{1+\gamma_1}{2}} - \left(\frac{c_3\tilde{\theta}^2}{2c_2}\right)^{\frac{1+\gamma_1}{2}} - \bar{\lambda}_3 V_2^{\frac{1+\gamma_2}{2}} \\ & - \frac{c\gamma_2}{c_2(1+\gamma_2)} \times (2c_2)^{\frac{1+\gamma_2}{2}} \times \left(\frac{\tilde{\theta}^2}{2c_2}\right)^{\frac{1+\gamma_2}{2}} + \vartheta_2 \\ \leq & -\mu_1 V_3^{\rho_1} - \mu_2 V_3^{\rho_2} + \vartheta_2, \end{aligned} \tag{52}$$

where $\vartheta_2 = \vartheta_1 + \Theta(\gamma_1) + \frac{c_3\theta^2}{2c_2} + \frac{c\gamma_2\theta^{1+\gamma_2}}{c_2(1+\gamma_2)}, \rho_1 = \frac{1+\gamma_1}{2}, \rho_2 = \frac{1+\gamma_2}{2}, \mu_1 = \min\{\bar{\lambda}_2, c_3^{\frac{1+\gamma_1}{2}}\}$, and $\mu_2 = \min\{\bar{\lambda}_3, \frac{c\gamma_2}{c_2(1+\gamma_2)} \times (2c_2)^{\frac{1+\gamma_2}{2}}\}$.

According to Lemma 1, it is concluded from (52) that the trajectory tracking error $z_{1,i}$ can converge into a sufficiently small region as follows:

$$\Delta = \left\{ \lim_{t\to T} z_1 \mid V_3 \leq \min\left(\left(\frac{\eta}{(1-\zeta)\mu_1}\right)^{\frac{1}{\rho_1}}, \left(\frac{\eta}{(1-\zeta)\mu_2}\right)^{\frac{1}{\rho_2}}\right)\right\}, \tag{53}$$

where $0 < \zeta < 1$, and the settling time T satisfies the following inequality as

$$T \leq T_{\max} \triangleq \frac{1}{\mu_1}\frac{1}{\zeta(\rho_1 - 1)} + \frac{1}{\varrho_2}\frac{1}{\zeta(1-\rho_2)}. \tag{54}$$

■

IV. SIMULATION

Let us consider a two-joint rigid robot manipulator [15], whose configuration is shown in Figure 1. Its dynamics in Lagrangian equation (1) are represented as follows:

$$M(q) = \begin{bmatrix} m_{11} & m_{1,2} \\ m_{21} & m_{22} \end{bmatrix}, C(q,\dot{q}) = \begin{bmatrix} c_{11} & c_{1,2} \\ c_{21} & c_{22} \end{bmatrix}, \tag{55}$$

$$G(q) = \begin{bmatrix} g_1, & g_2 \end{bmatrix}^T, \boldsymbol{d}(t) = \begin{bmatrix} d_1, & d_2 \end{bmatrix}^T, \tag{56}$$

with

$$\begin{aligned} q &= [q_1, q_2]^T, \\ m_{11} &= (m_1 + m_2)l_1^2 + m_2 l_2^2 + 2m_2 l_1 l_2 \cos(q_2) + J_1, \\ m_{1,2} &= m_2 l_2^2 + m_2 l_1 l_2 \cos(q_2), \\ m_{21} &= m_2 l_2^2 + m_2 l_1 l_2 \cos(q_2), \\ m_{22} &= m_2 l_2^2 + J_2, \\ c_{11} &= -m_2 l_1 l_2 \sin(q_2)\dot{q}_2, \\ c_{1,2} &= -m_2 l_1 l_2 \sin(q_2)(\dot{q}_1 + \dot{q}_2), \\ c_{21} &= m_2 l_1 l_2 \sin(q_2)\dot{q}_1, \\ c_{22} &= 0, \\ g_1 &= (m_1 + m_2)l_1 g \cos(q_1) + m_2 l_2 g \cos(q_1 + q_2), \\ g_2 &= m_2 l_2 g \cos(q_1 + q_2). \end{aligned} \tag{57}$$

The real values of model parameters and disturbances are taken as $l_1 = 1.0$ m, $l_2 = 0.8$ m, $m_1 = 1.5$kg, $m_2 = 0.5$kg, $J_1 = 5$kg.m^2, $J_2 = 5$kg.m^2, $g = 9.8$m/s^2, $d_1(t) = 0.5\sin(200\pi t) + 2\sin(t)$ N · m and $d_2(t) = 0.5\sin(200\pi t) + \cos(2t)$ N · m, which are unknown during controller design. The nominal values of m_1 and m_2 are 1.2kg and 0.4kg, respectively. The reference signals are given as $q_{1d} = 1.25 - 1.4\mathrm{e}^{-t} + 0.35\mathrm{e}^{-4t}$ rad and $q_{2d} = 1.25 + \mathrm{e}^{-t} - 0.25\,\mathrm{e}^{-4t}$ rad. The maximum allowable torque are set as $u_{1\max} = 30$ N · m.

To effectively verify the convergence performance of SFFTNAC approach, two different initial conditions of robot manipulator are considered as follows:

Case 1): $q_1(0) = 1$ rad, $q_2(0) = 0.5$ rad, $\dot{q}_1(0) = 0$ rad/s and $\dot{q}_2(0) = 0$ rad/s;

Case 2): $q_1(0) = 0.8$ rad, $q_2(0) = 0.8$ rad, $\dot{q}_1(0) = 0$ rad/s and $\dot{q}_2(0) = 0$ rad/s.

In the proposed strategy, the parameters of virtual controller (21) and (23), fixed-time controller (35) and (37), and adaptive law (38) are set as $k_1 = 1, k_2 = 2, k_3 = 2, \lambda_1 = 1, \lambda_2 = 2, \lambda_3 = 2, \gamma_1 = \frac{5}{9}, \gamma_2 = \frac{7}{5}, c_1 = 1, c_2 = 0.5, c_3 = 1, c_4 = 1, \varpi_1 = 0.001, \varpi_2 = 0.001$. Besides, the parameters of sigmoid function in (34) are set as $\varsigma_1 = 6, \varsigma_2 = 8, \varsigma_3 = 12, \varsigma_4 = 0.1$.

The simulation results are provided in Figures 2-13. The angular positions of Joint 1 in two cases are respectively shown in Fig. 2 and Fig. 4, from which we can see that the angular position convergence time in Case 1 of Joint 1 is almost the same as that in Case 2 of Joint 1. Similarly, from Fig. 3 and Fig. 5, we can see that the angular position convergence time in Case 1 of Joint 2 is almost the same as

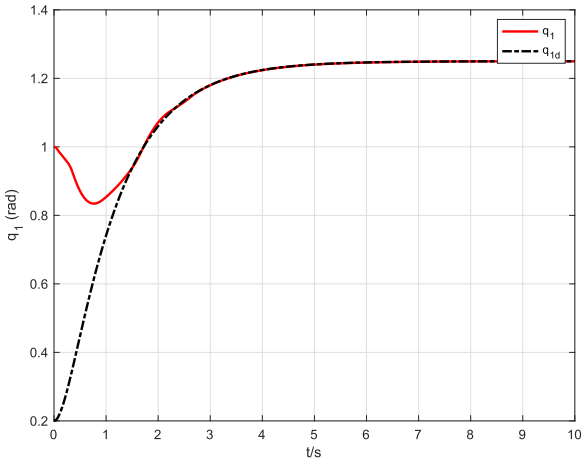

FIGURE 2. The angular position of joint 1 (Case 1, SFFTNAC).

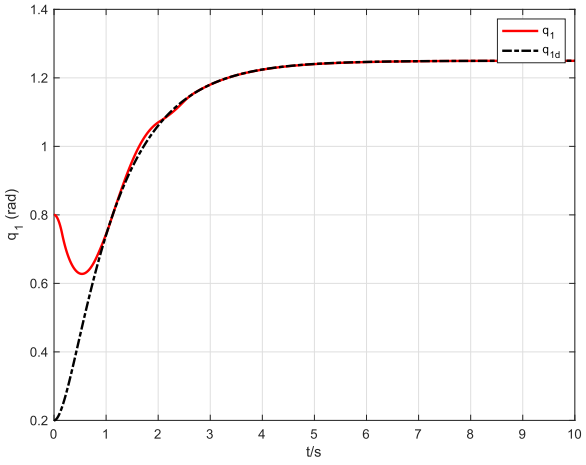

FIGURE 3. The angular position of joint 1 (Case 2, SFFTNAC).

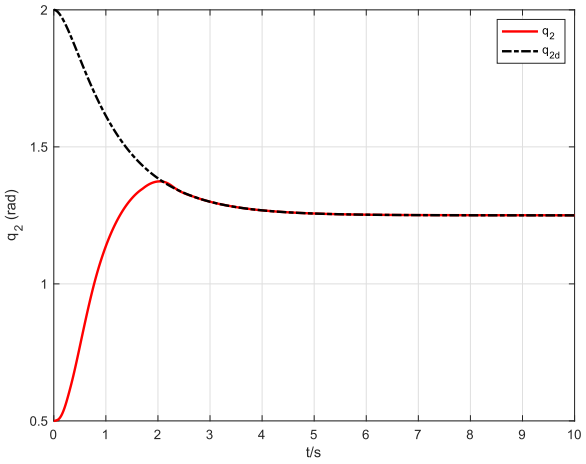

FIGURE 4. The angular position of joint 2 (Case 1, SFFTNAC).

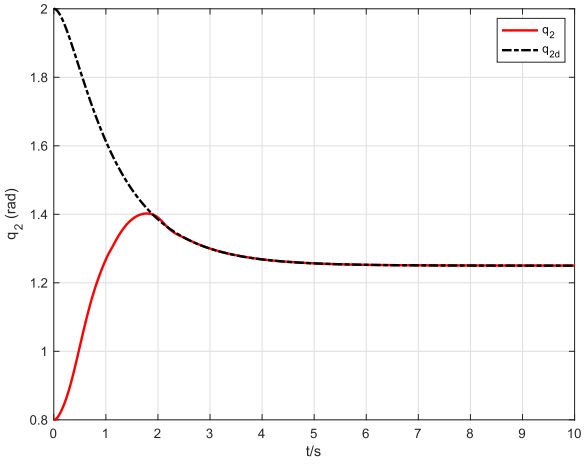

FIGURE 5. The angular position of joint 2 (Case 2, SFFTNAC).

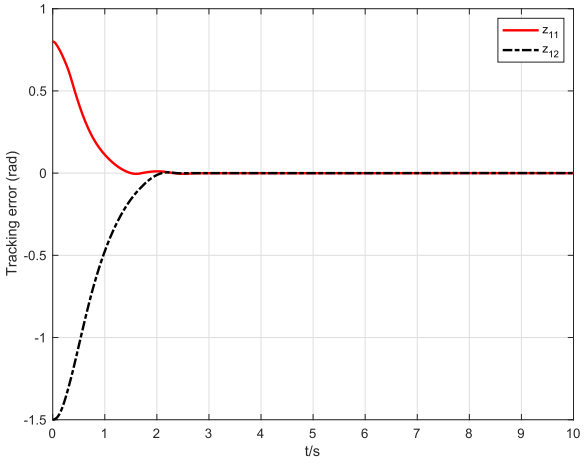

FIGURE 6. The angular position error signal $\boldsymbol{z}_1$ (Case 1, SFFTNAC).

that in Case 2 of Joint 2. Hence, we can draw a conclusion that the upper bound convergence time of our control scheme is irrelevant to different initial conditions. The angular position error signal $\boldsymbol{z}_1$ and the intermediate error signal $\boldsymbol{z}_2$ in two cases are shown in Figures 6-9. From them, it can be seen that the upper bound convergence time of proposed control strategy in Case 1 and Case 2 is about 2.5 second, which is independent of initial conditions. Figure 10 and Figure 11 display the parameter estimation of $\hat{\theta}$ under different initial values. We can see that $\hat{\theta}$ can converge to constants over time, which indicates the good compensation for uncertainties has been obtained in the robotic system. Finally, the control torque under different initial values are shown in Figs, 12-13, from which we can see the profiles of control torque are smooth and continuous in the time domain while the saturation property is guaranteed during the operation of control system.

To further demonstrate the advantage of our proposed control scheme, a nonsingular fast terminal sliding mode control (NSFTSMC) algorithm is introduced [38] for comparison as follows:

$$\boldsymbol{\tau} = -M_0\big[\varsigma_2 \boldsymbol{S}_\Sigma + (\rho+\varsigma_1)\frac{\boldsymbol{S}_\Sigma}{\|\boldsymbol{S}_\Sigma\|+\delta} + \boldsymbol{F} + \Gamma_2^{-1}(I_2 + \Gamma_1 \mathrm{diag}(|\boldsymbol{z}_1|^{\Gamma_1 - I_2}))\mathrm{sign}^{2I_2-\Gamma_2}(\dot{\boldsymbol{z}}_1), \tag{58}$$

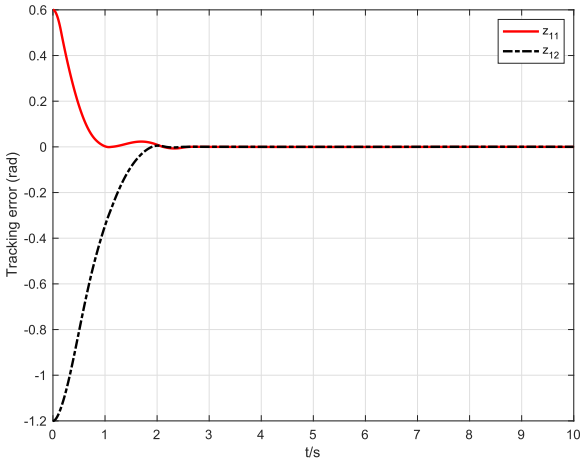

FIGURE 7. The angular position error signal $\boldsymbol{z}_1$ (Case 2, SFFTNAC).

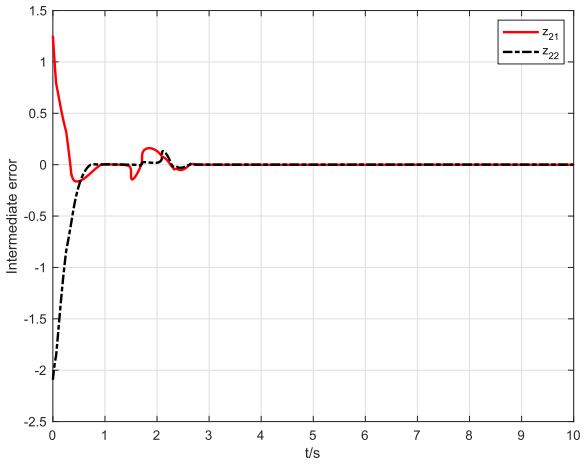

FIGURE 8. The intermediate error signals $\boldsymbol{z}_2$ (Case 1, SFFTNAC).

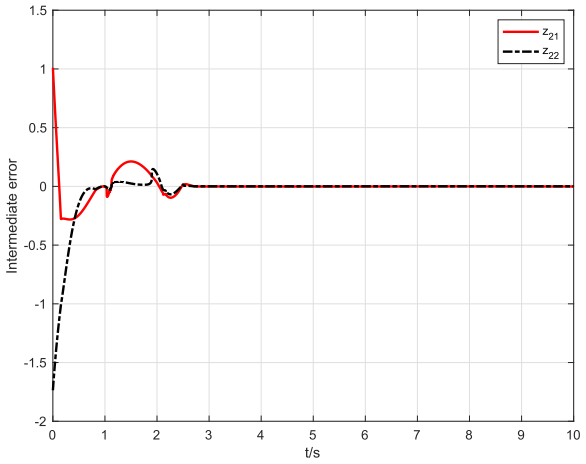

FIGURE 9. The intermediate error signals $\boldsymbol{z}_2$ (Case 2, SFFTNAC).

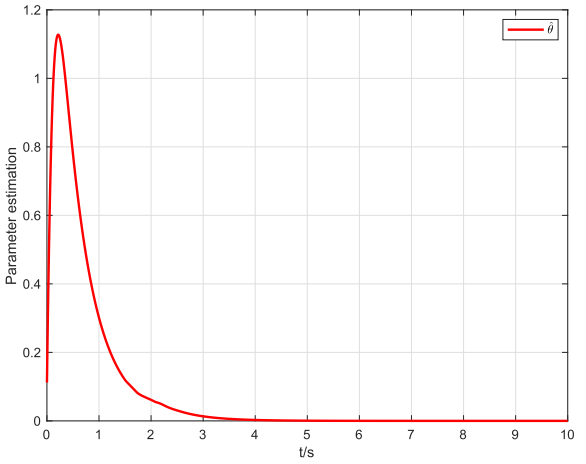

FIGURE 10. The estimated parameter $\hat{\theta}$ (Case 1, SFFTNAC).

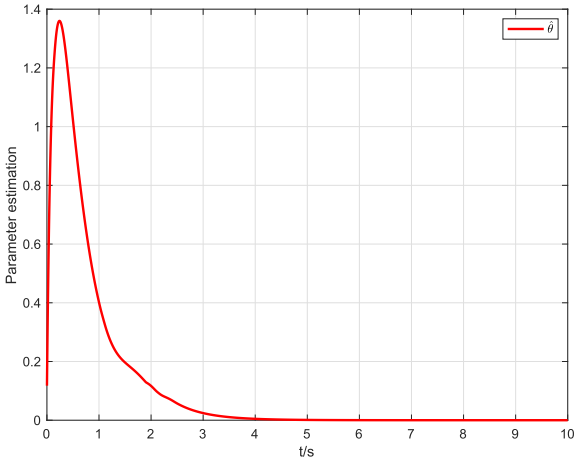

FIGURE 11. The estimated parameter $\hat{\theta}$ (Case 2, SFFTNAC).

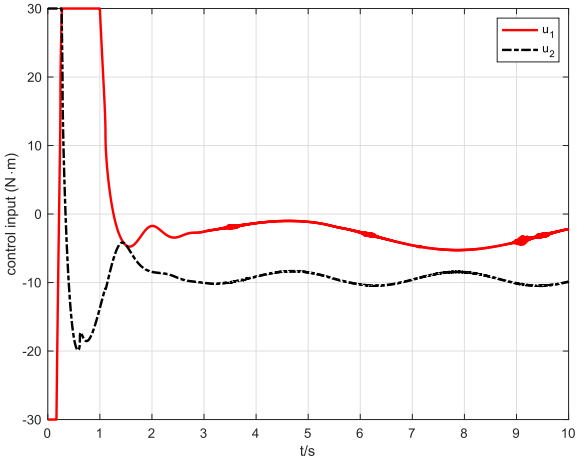

FIGURE 12. The control torque $\boldsymbol{u}$ (Case 1, SFFTNAC).

where $\boldsymbol{S}_\Sigma = \boldsymbol{z}_1 + \text{sign}^{\Gamma_1}(\boldsymbol{z}_1) + \text{sign}^{\Gamma_2}(\dot{\boldsymbol{z}}_1)$, $\boldsymbol{F} = -M_0^{-1}(\boldsymbol{q})(C_0(\boldsymbol{q},\dot{\boldsymbol{q}})\dot{\boldsymbol{q}}+\boldsymbol{G}_0(\boldsymbol{q}))-\ddot{\boldsymbol{q}}_d$, $\rho = \|M_0^{-1}\|(b_0+b_1\|\boldsymbol{q}\|+b_2\|\dot{\boldsymbol{q}}\|^2)$, with $b_0 = 2, b_1 = 0.5, b_2 = 0.3$, $\varsigma_1 = 1$, $\varsigma_2 = 2, \delta = 0.01$,

$$\Gamma_1 = \begin{bmatrix} 2 & 0 \\ 0 & 2 \end{bmatrix}, \Gamma_2 = \begin{bmatrix} \frac{5}{3} & 0 \\ 0 & \frac{5}{3} \end{bmatrix}, I_2 = \begin{bmatrix} 1 & 0 \\ 0 & 1 \end{bmatrix}. \quad (59)$$

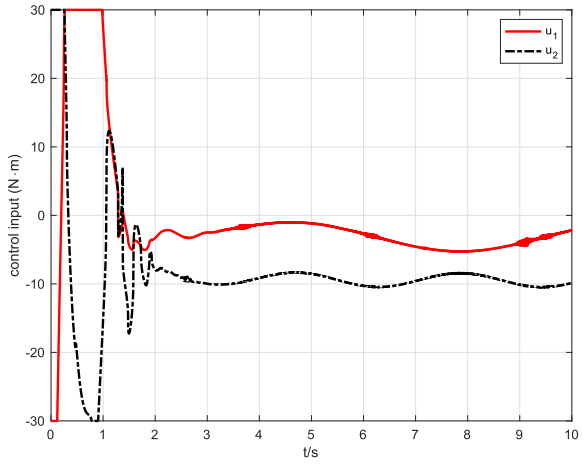

FIGURE 13. The control torque $\boldsymbol{u}$ (Case 2, SFFTNAC).

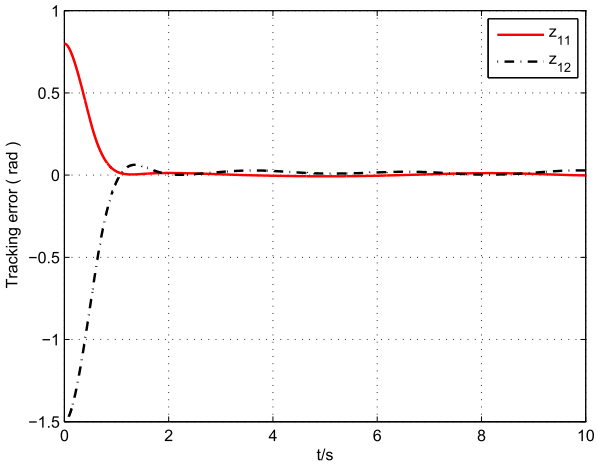

FIGURE 16. The angular position error $\boldsymbol{z}_1$ (Case 1, NSFTSMC).

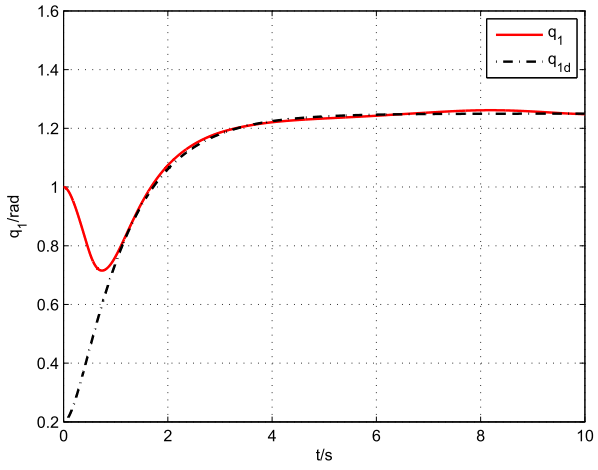

FIGURE 14. The angular position of joint 1 (Case 1, NSFTSMC).

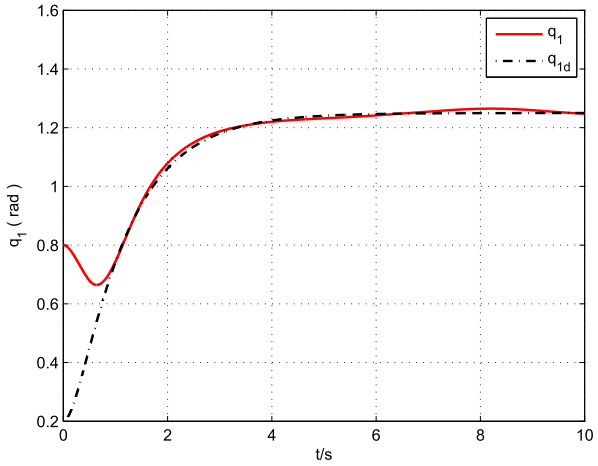

FIGURE 17. The angular position of joint 1 (Case 2, NSFTSMC).

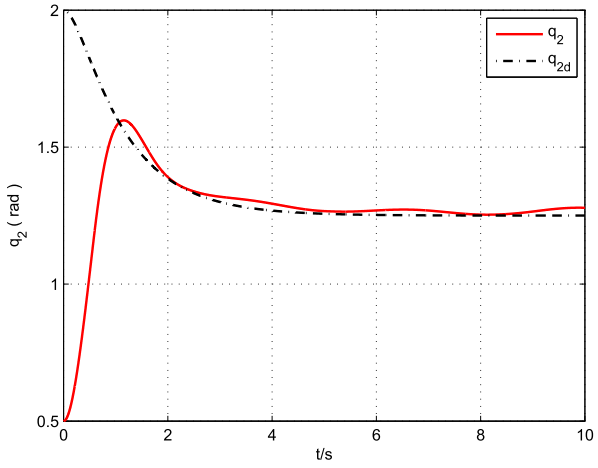

FIGURE 15. The angular position of joint 2 (Case 1, NSFTSMC).

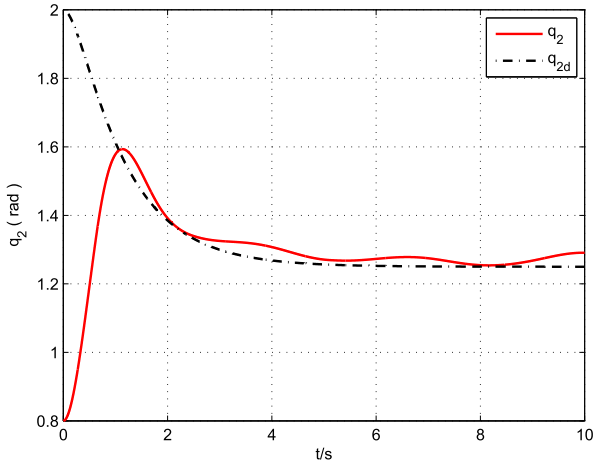

FIGURE 18. The angular position of joint 2 (Case 2, NSFTSMC).

The angular position tracking response of Joint 1 in two Cases are respectively shown in Fig. 14 and Fig. 17, while the angular position tracking response of Joint 2 in two Cases are respectively shown in Fig. 15 and Fig. 18. The tracking error profiles are shown in Fig. 16 and Fig. 19. Comparing Figs. 2,4,6 and Figs. 14, 15,16, we can see that better control precision may be obtained in Case 1 of SFFTNAC system. Similarly, through comparing Figs. 3,5,7 and Figs. 17, 18,19,

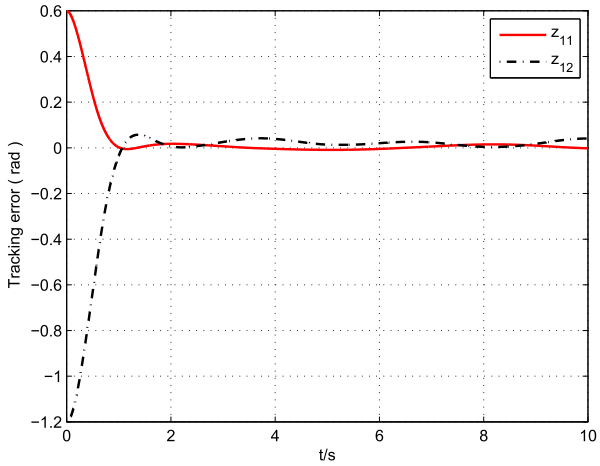

FIGURE 19. The angular position error z_1 (Case 2, NSFTSMC).

it can be found that in Case 2, the robot manipulator system under SFFTNAC possesses better steady-state performance than the one under NSFTSMC. From Figs. 16 and 19, we can see that the NSFTSMC system does not meet the property of fixed-time convergence. It is worth noting that in NSFTSMC scheme, we can get higher control precision by letting the parameter δ sufficiently small, nevertheless the chattering phenomenon tends to occur if δ is set too small.

The above results confirm that, compared with the NSFTSMC scheme, the proposed SFFTNAC scheme can achieve superior tracking performance for a robot manipulator system, with faster convergence speed and higher tracking accuracy. Additionally, the convergence time of the proposed SFFTNAC scheme is independent of the system's initial conditions.

V. CONCLUSION

This article has addressed the singularity-free fixed-time neuro-adaptive control problem for trajectory tracking in robot manipulators with model uncertainties, external disturbances, and input saturation. The proposed singularity-free fixed-time neuro-adaptive controller ensures that the settling time of the robot system is independent of the initial states and can be estimated in advance. In comparison to existing fixed-time control schemes, singularity avoidance is achieved by constructing quadratic-fraction functions in the virtual controller, eliminating the need for filters or piecewise continuous functions. Finally, the simulations have been provided to demonstrate that the effectiveness of the proposed singularity-free fixed-time neuro-adaptive control strategy. In the future, we will focus on output-constraint fixed-time control and prescribed-time fault-tolerant control for robot manipulators.

REFERENCES

[1] Q. Hu, C. Guo, Y. Zhang, and J. Zhang, "Recursive decentralized control for robot manipulators," *Aerosp. Sci. Technol.*, vol. 76, pp. 374–385, May 2018.

[2] K. Kreutz, "On manipulator control by exact linearization," *IEEE Trans. Autom. Control*, vol. 34, no. 7, pp. 763–767, Jul. 1989.

[3] J. Alvarez-Ramirez, I. Cervantes, and R. Kelly, "PID regulation of robot manipulators: Stability and performance," *Syst. Control Lett.*, vol. 41, no. 2, pp. 73–83, Oct. 2000.

[4] D.-J. Lee, Y. Park, and Y.-S. Park, "Robust H_∞ sliding mode descriptor observer for fault and output disturbance estimation of uncertain systems," *IEEE Trans. Autom. Control*, vol. 57, no. 11, pp. 2928–2934, Nov. 2012.

[5] S. Islam and P. X. Liu, "Robust adaptive fuzzy output feedback control system for robot manipulators," *IEEE/ASME Trans. Mechatronics*, vol. 16, no. 2, pp. 288–296, Apr. 2011.

[6] Y. H. Kim and F. L. Lewis, "Neural network output feedback control of robot manipulators," *IEEE Trans. Robot. Autom.*, vol. 15, no. 2, pp. 301–309, Apr. 1999.

[7] W. He and Y. Dong, "Adaptive fuzzy neural network control for a constrained robot using impedance learning," *IEEE Trans. Neural Netw. Learn. Syst.*, vol. 29, no. 4, pp. 1174–1186, Apr. 2018.

[8] J. Baek, M. Jin, and S. Han, "A new adaptive sliding-mode control scheme for application to robot manipulators," *IEEE Trans. Ind. Electron.*, vol. 63, no. 6, pp. 3628–3637, Jun. 2016.

[9] S. P. Bhat and D. S. Bernstein, "Continuous finite-time stabilization of the translational and rotational double integrators," *IEEE Trans. Autom. Control*, vol. 43, no. 5, pp. 678–682, May 1998.

[10] Z. Zuo and L. Tie, "Distributed robust finite-time nonlinear consensus protocols for multi-agent systems," *Int. J. Syst. Sci.*, vol. 47, no. 6, pp. 1366–1375, Apr. 2016.

[11] X. Zheng, X. Yu, J. Jiang, and X. Yang, "Practical finite-time command filtered backstepping with its application to DC motor control systems," *IEEE Trans. Ind. Electron.*, vol. 71, no. 3, pp. 2955–2964, Mar. 2024.

[12] X. Zheng, X. Yu, X. Yang, and J. J. Rodriguez-Andina, "Practical finite-time command-filtered adaptive backstepping with its applications to quadrotor hovers," *IEEE Trans. Cybern.*, pp. 1–13, 2023, doi: 10.1109/TCYB.2023.3323664.

[13] S. Xie, M. Tao, Q. Chen, and L. Tao, "Neural-network-based adaptive finite-time output constraint control for rigid spacecrafts," *Int. J. Robust Nonlinear Control*, vol. 32, no. 5, pp. 2983–3000, Mar. 2022.

[14] K. Li and Y. Li, "Adaptive neural network finite-time dynamic surface control for nonlinear systems," *IEEE Trans. Neural Netw. Learn. Syst.*, vol. 32, no. 12, pp. 5688–5697, Dec. 2021.

[15] S. Yu, X. Yu, and B. Shirinzadeh, "Continuous finite-time control for robot manipulators with terminal sliding mode," *Automatica*, vol. 41, no. 11, pp. 1957–1964, 2005.

[16] F. Luan, J. Na, Y. Huang, and G. Gao, "Adaptive neural network control for robotic manipulators with guaranteed finite-time convergence," *Neurocomputing*, vol. 337, pp. 153–164, Apr. 2019.

[17] J. Zhai and G. Xu, "A novel non-singular terminal sliding mode trajectory tracking control for robotic manipulators," *IEEE Trans. Circuits Syst. II, Exp. Briefs*, vol. 68, no. 1, pp. 391–395, Jan. 2021.

[18] A. Polyakov, "Nonlinear feedback design for fixed-time stabilization of linear control systems," *IEEE Trans. Autom. Control*, vol. 57, no. 8, pp. 2106–2110, Aug. 2012.

[19] Z. Zuo, "Nonsingular fixed-time consensus tracking for second-order multi-agent networks," *Automatica*, vol. 54, pp. 305–309, Apr. 2015.

[20] Q. Chen, S. Xie, M. Sun, and X. He, "Adaptive nonsingular fixed-time attitude stabilization of uncertain spacecraft," *IEEE Trans. Aerosp. Electron. Syst.*, vol. 54, no. 6, pp. 2937–2950, Dec. 2018.

[21] M. Van and D. Ceglarek, "Robust fault tolerant control of robot manipulators with global fixed-time convergence," *J. Franklin Inst.*, vol. 358, no. 1, pp. 699–722, Jan. 2021.

[22] L. Zhang, H. Liu, D. Tang, Y. Hou, and Y. Wang, "Adaptive fixed-time fault-tolerant tracking control and its application for robot manipulators," *IEEE Trans. Ind. Electron.*, vol. 69, no. 3, pp. 2956–2966, Mar. 2022.

[23] Z. Gao and G. Guo, "Command-filtered fixed-time trajectory tracking control of surface vehicles based on a disturbance observer," *Int. J. Robust Nonlinear Control*, vol. 29, no. 13, pp. 4348–4365, Sep. 2019.

[24] Q. Yang, Z. Yang, and Y. Sun, "Universal neural network control of MIMO uncertain nonlinear systems," *IEEE Trans. Neural Netw. Learn. Syst.*, vol. 23, no. 7, pp. 1163–1169, Jul. 2012.

[25] D.-P. Li, Y.-J. Liu, S. Tong, C. L. P. Chen, and D.-J. Li, "Neural networks-based adaptive control for nonlinear state constrained systems with input delay," *IEEE Trans. Cybern.*, vol. 49, no. 4, pp. 1249–1258, Apr. 2019.

[26] C. Liu, H. Wang, X. Liu, and Y. Zhou, "Adaptive finite-time fuzzy funnel control for nonaffine nonlinear systems," *IEEE Trans. Syst., Man, Cybern. Syst.*, vol. 51, no. 5, pp. 2894–2903, May 2021.

[27] Y.-X. Li, X. Hu, W. Che, and Z. Hou, "Event-based adaptive fuzzy asymptotic tracking control of uncertain nonlinear systems," *IEEE Trans. Fuzzy Syst.*, vol. 29, no. 10, pp. 3003–3013, Oct. 2021.
[28] W. He, Y. Chen, and Z. Yin, "Adaptive neural network control of an uncertain robot with full-state constraints," *IEEE Trans. Cybern.*, vol. 46, no. 3, pp. 620–629, Mar. 2016.
[29] L. Wang, T. Chai, and L. Zhai, "Neural-network-based terminal sliding-mode control of robotic manipulators including actuator dynamics," *IEEE Trans. Ind. Electron.*, vol. 56, no. 9, pp. 3296–3304, Sep. 2009.
[30] Y. Zhang, C. Hua, and K. Li, "Disturbance observer-based fixed-time prescribed performance tracking control for robotic manipulator," *Int. J. Syst. Sci.*, vol. 50, no. 13, pp. 2437–2448, Oct. 2019.
[31] Y. Zhu, J. Qiao, and L. Guo, "Adaptive sliding mode disturbance observer-based composite control with prescribed performance of space manipulators for target capturing," *IEEE Trans. Ind. Electron.*, vol. 66, no. 3, pp. 1973–1983, Mar. 2019.
[32] M. Chen, H. Wang, and X. Liu, "Adaptive fuzzy practical fixed-time tracking control of nonlinear systems," *IEEE Trans. Fuzzy Syst.*, vol. 29, no. 3, pp. 664–673, Mar. 2021.
[33] L.-X. Wang and J. M. Mendel, "Fuzzy basis functions, universal approximation, and orthogonal least-squares learning," *IEEE Trans. Neural Netw.*, vol. 3, no. 5, pp. 807–814, Sep. 1992.
[34] Y. Sun and L. Zhang, "Fixed-time adaptive fuzzy control for uncertain strict feedback switched systems," *Inf. Sci.*, vol. 546, pp. 742–752, Feb. 2021.
[35] T. Zhang, "Adaptive neural network control for strict-feedback nonlinear systems using backstepping design," *Automatica*, vol. 36, no. 12, pp. 1835–1846, Dec. 2000.
[36] J. Yu, P. Shi, W. Dong, B. Chen, and C. Lin, "Neural network-based adaptive dynamic surface control for permanent magnet synchronous motors," *IEEE Trans. Neural Netw. Learn. Syst.*, vol. 26, no. 3, pp. 640–645, Mar. 2015.
[37] G. Feng, "A compensating scheme for robot tracking based on neural networks," *Robot. Auton. Syst.*, vol. 15, no. 3, pp. 199–206, Aug. 1995.
[38] L. Yang and J. Yang, "Nonsingular fast terminal sliding-mode control for nonlinear dynamical systems," *Int. J. Robust Nonlinear Control*, vol. 21, no. 16, pp. 1865–1879, Nov. 2011.

DONG GUO received the M.Eng. degree from Hangzhou Dianzi University, Hangzhou, China, in 2013, where he is currently pursuing the Ph.D. degree in control science and engineering. He is with the School of Electrical Engineering, Zhejiang University of Water Resources and Electric Power. His research interests include electronic technology, sensing technology, and adaptive control.

JUN LIU received the B.Eng. and M.Eng. degrees from the School of Automation (Artificial Intelligence), Hangzhou Dianzi University, Hangzhou, China, in 2013 and 2016, respectively, and the Ph.D. degree from the College of Control Science and Engineering, Zhejiang University, Hangzhou. He is currently a Lecturer with the School of Information Science and Technology, Hangzhou Normal University, Hangzhou. His research interests include artificial intelligence, machine learning, process monitoring, vehicle emission monitoring, unmanned autonomous systems, and sensor networks.

SONG ZHENG was born in 1982. He received the Ph.D. degree from the College of Control Science and Engineering, Zhejiang University, Hangzhou, in 2008. He is currently an Associate Professor with the School of Automation (Artificial Intelligence), Hangzhou Dianzi University. His main research interests include system modeling and optimizing, and integrated automation systems.

JIAN-PING CAI was born in 1975. He received the Ph.D. degree from Zhejiang University, in 2014. He is currently a Professor with the Zhejiang University of Water Resources and Electric Power. His main research interests include nonlinear systems and adaptive control.

PENG JIANG received the B.Eng. and Ph.D. degrees from the College of Control Science and Engineering, Zhejiang University, Hangzhou, China, in 1999 and 2004, respectively. He is currently a Professor with the School of Information Science and Technology, Hangzhou Normal University, Hangzhou. His research interests include sensor networks, machine learning, artificial intelligence, vehicle emission monitoring, unmanned autonomous systems, and industrial safety.